American Mineralogist, Volume 74, pages 339–351, 1989

High-temperature cation distributions in Fe_3O_4-$MgAl_2O_4$-$MgFe_2O_4$-$FeAl_2O_4$ spinels from thermopower and conductivity measurements

JOHAN NELL, BERNARD J. WOOD
Department of Geological Sciences, Northwestern University, Evanston, Illinois 60208, U.S.A.
THOMAS O. MASON
Department of Materials Science and Engineering, The Technological Institute, Northwestern University, Evanston, Illinois 60208, U.S.A.

ABSTRACT

The distribution of cations between octahedral and tetrahedral sites in Fe_3O_4-$FeAl_2O_4$, Fe_3O_4-$MgFe_2O_4$, and Fe_3O_4-$MgAl_2O_4$ solid solutions has been determined in situ at 600 °C to 1400 °C and 1-atm pressure. The method uses a combination of thermopower and electrical conductivity measurements to characterize the partitioning of Fe^{2+} and Fe^{3+} between the two sites. This enables determination of all cation occupancies on the Fe_3O_4-$FeAl_2O_4$ and Fe_3O_4-$MgFe_2O_4$ joins, but requires use of a model to fix one other parameter in Fe_3O_4-$MgAl_2O_4$ solid solutions.

The data have been used to evaluate the applicability of currently used cation-distribution models to spinels. The join Fe_3O_4-$MgFe_2O_4$ fits reasonably well to either the simple constant $K_{Cd}^{Fe^{2+}\text{-}Fe^{3+}}$ and $K_{Cd}^{Mg\text{-}Fe^{3+}}$ model (Navrotsky and Kleppa, 1967) or to the more complex O'Neill-Navrotsky (1983, 1984) model in which $-RT \ln K_{Cd}$ is predicted to be a linear function of the occupancy of tetrahedral sites by trivalent cations. Cation-distribution data for Fe_3O_4-$FeAl_2O_4$ solid solutions are in quantitative agreement with the O'Neill-Navrotsky model in that $-RT \ln K_{Cd}^{Fe^{2+}\text{-}Fe^{3+}}$ and $-RT \ln K_{Cd}^{Fe^{2+}\text{-}Al}$ are linear functions of the degree of inversion. The observed variations of $-RT \ln K_{Cd}^{Fe^{2+}\text{-}Al}$ do not, however, agree with those in end-member hercynite so that this join only agrees qualitatively with the model. Fe_3O_4-$MgAl_2O_4$ solutions are intermediate in behavior between the other two joins, their cation distributions ($-RT \ln K_{Cd}^{Fe^{2+}\text{-}Fe^{3+}}$, $-RT \ln K_{Cd}^{Fe^{2+}\text{-}Al}$, and $-RT \ln K_{Cd}^{Mg\text{-}Fe^{2+}}$) being linear functions of tetrahedral trivalent ions and in broad agreement with the data for pure magnetite, hercynite, and magnesioferrite, respectively.

INTRODUCTION

Spinels are important constituents of many igneous and metamorphic rocks as well as furnace smelting products. They are also of interest to the ceramic industry mainly because of their magnetic properties. Spinel equilibria have been widely used as petrogenetic indicators (e.g., Sack, 1982; Buddington and Lindsley, 1964; Gasparik and Newton, 1984), but most of these calibrations are limited in application because phase-equilibrium experiments are generally performed only over a narrow temperature range. In spinels, disordering between octahedral and tetrahedral sites greatly influences the partial molar entropies of components and hence the temperature dependencies of activities and interphase partitioning. Therefore, it is necessary to characterize the order-disorder phenomena adequately in order to have confidence in the extrapolation of thermobarometric calibrations outside the experimental temperature ranges. Cation distributions determined on quenched samples are, however, subject to considerable uncertainty because of the tendency for re-ordering during cooling (O'Neill and Navrotsky, 1983). A high-temperature in-situ method is therefore needed to precisely characterize order-disorder phenomena in spinels.

It was shown by Wu et al. (1981) that the thermoelectric coefficient could be used to measure cation distributions in ferrospinels at elevated temperatures when only two cations (e.g., Fe^{3+} and Fe^{2+}) are interchanged between octahedral and tetrahedral sites. This method has subsequently been successfully applied to determine cation distributions in Fe_3O_4 (Wu and Mason, 1981) and the Fe_3O_4-Fe_2TiO_4 solid-solution series where it may be assumed that all the Ti is in octahedral coordination (Trestman-Matts et al., 1983). A more complex case was studied by Trestman-Matts et al. (1984), who measured the thermoelectric coefficient in Fe_3O_4-$MgFe_2O_4$ spinels as a function of temperature. In this system, all three cations (Mg, Fe^{2+}, and Fe^{3+}) are disordered between the two sites, and Trestman-Matts et al. had to use a Mg-Fe^{3+} site-preference energy (obtained from the degree of inversion of pure $MgFe_2O_4$), in addition to the measured ratio of Fe^{3+}/Fe^{2+} on the octahedral site, to calculate the distributions of all cations in the solid solution. Mason (1985) used a similar strategy to determine cation distributions in Fe_3O_4-$FeAl_2O_4$ spinels at 1700 K.

0003–004X/89/0304–0339$02.00

Mason (1987) showed that the use of conductivity measurements in conjunction with thermopower measurements would, at high temperature, enable complete characterization of cation distributions in ferrospinel solid solutions in which three cations disorder between octahedral and tetrahedral sites. This method obviates the need for a distribution model for one of the cations. In this study we have measured both thermopower and conductivity in Fe_3O_4-$FeAl_2O_4$, Fe_3O_4-$MgFe_2O_4$, and Fe_3O_4-$MgAl_2O_4$ solid solutions over the temperature range 600 to 1400 °C. The technique of Mason (1987) enables the complete calculation of cation distributions in the Fe_3O_4-$MgFe_2O_4$ and Fe_3O_4-$FeAl_2O_4$ systems as a function of temperature. In the Fe_3O_4-$MgAl_2O_4$ solid solution, however, four cations (Fe^{2+}, Fe^{3+}, Mg, and Al) disorder over the two sites, and a Mg-Al site-preference energy (Wood et al., 1986) must be used in addition to the measured Fe^{2+}-Fe^{3+} distribution in order to solve for all intersite cation distributions. The latter join is of considerable petrologic importance because of its calibration as an oxygen barometer for ultramafic rocks (Mattioli and Wood, 1988).

Thermopower-conductivity theory

Extensive reviews of cation-distribution theory in ferrospinels and the application of thermopower and conductivity measurements to the determination of intersite cation distributions are given by Wu et al. (1981) and Mason (1987). The structural formula for mixtures of Fe_3O_4, $FeAl_2O_4$, $MgFe_2O_4$, and $MgAl_2O_4$ may be written as

$$Fe_a^{2+}Fe_b^{3+}Mg_mAl_n(Fe_d^{2+}Fe_e^{3+}Mg_oAl_p)O_4, \quad (1)$$

where the species in parentheses reside on the octahedral sites and the remainder in tetrahedral positions.

Provided small polaron conduction is operative, thermopower measurements can be used to calculate the octahedral valence ratio, $q = (Fe^{3+}/Fe^{2+})_{oct} = e/d$ from the thermoelectric coefficient (Q, in VK^{-1}) according to (Wu and Mason, 1981)

$$Q = \frac{-k}{e_0}\left[\ln\left(\beta\frac{1-c}{c}\right) + A\right], \quad (2)$$

where k is Boltzmann's constant, e_0 is the electronic charge, β is a spin-degeneracy term found to be equal to 2 (Mason and Bowen, 1981), and A is an entropy-of-vibration term that is negligibly small in the case of small polaron conduction (Wu and Mason, 1981). The ratio $(1 - c)/c$ corresponds to the ratio of Fe cations on the conducting sites, where the variable c represents the fraction of conducting sites of lower valence (Fe^{2+}) and $(1 - c)$ the fraction of Fe^{3+}. In magnetite solid solutions, this ratio is equivalent to the octahedral valence ratio since it has been shown in many studies that small polaron conduction is restricted to the octahedral sites in ferrospinels (e.g., Kuendig and Hargrove, 1969; Mason, 1987). Equation 2 may be rearranged to obtain the octahedral valence ratio

$$q = Fe^{3+}/Fe^{2+} = e/d = \tfrac{1}{2}\exp(-Qe_0/k). \quad (3)$$

In order to solve explicitly for the intersite distribution of Fe species in Fe_3O_4-$MgFe_2O_4$, Fe_3O_4-$FeAl_2O_4$, and Fe_3O_4-$MgAl_2O_4$ solid solutions, it is also necessary to be able to measure the total concentrations of Fe^{3+} and Fe^{2+} on either the tetrahedral or octahedral sites. This may be achieved by measuring the electrical conductivity since the latter depends on the sum of Fe species participating in conduction.

The electrical conductivity [in $(\Omega\cdot cm)^{-1}$] in the case of a small polaron conductor is given by (Tuller and Nowick, 1977; Dieckmann et al., 1983)

$$\sigma = \frac{gNc'(1-c')e_0^2a^2\nu_0}{kT}\exp\left(\frac{-E_H}{kT}\right), \quad (4)$$

where g is a geometrical factor involving coordination number (constant for a given system), N is the density of conducting sites in cm^{-3}, c' is the fraction of conducting sites occupied by charge carriers, $(1 - c')$ is the fraction of available jump sites (Fe^{2+} and Fe^{3+}, respectively, in the case of an n-type small polaron conductor), a is the jump distance (cm), ν_0 is the lattice vibrational frequency responsible for conduction, E_H is the hopping energy, and T = temperature. For an octahedral small polaron process, $c' = d/(d + e) = 1/(1 + q)$ and $(1 - c') = e/(e + d) = q/(1 + q)$, where q is the previously defined octahedral valence ratio. In principle, of course, Equation 4 may only be applied to solve for one parameter (N, for example), and the remainder should be known. In order to apply the equation therefore, a simplification is necessary. Mason (1987) suggested that a and ν_0 should be essentially composition-independent in a given solid solution, in which case we obtain for N, the density of conducting sites (in cm^{-3}),

$$N = \frac{(\text{constant})T\sigma}{c'(1-c')\exp(-E_H/kT)}. \quad (5)$$

Taking the ratio of N between a solid-solution composition (x_n) and magnetite (x_1) at a fixed temperature then gives

$$\frac{N_{(x_n)}}{N_{(x_1)}} = \frac{\sigma_{(x_n)}[c'(1-c')]_{(x_1)}}{\sigma_{(x_1)}[c'(1-c')]_{(x_n)}}\exp\left(\frac{E_{H_{(x_n)}} - E_{H_{(x_1)}}}{kT}\right). \quad (6)$$

In order to calculate the exponential term in Equation 6, $\ln \sigma T$ is plotted versus $1/T$, thereby providing the apparent hopping energy (E_a). Mason (1987) showed that the difference in actual hopping energy between a solid-solution composition and pure magnetite is generally given by the difference in apparent hopping energies

$$E_{a_{(x_n)}} - E_{a_{(x_1)}} = E_{H_{(x_n)}} - E_{H_{(x_1)}}. \quad (7)$$

Therefore, with the measurement of σ and q, the value of N for the solid solution may be calculated provided N is known for pure magnetite. In the latter case, N is equal to the number of octahedral sites per formula unit, 2.

Experimental methods

Polycrystalline specimens with the compositions x = 0.25, 0.5, 0.75, and 1.0 in $Fe^{2+}Fe^{3+}_{2x}Al_{2-2x}O_4$, $Fe^{2+}_xMg_{1-x}Fe^{3+}_2O_4$, and $Fe^{2+}_xMg_{1-x}Fe^{3+}_{2x}Al_{2-2x}O_4$, were sintered from powders by repeated cycles of firing and grinding of oxide mixes in a controlled gas atmosphere. Starting materials were reagent-grade Fe_2O_3, $Al(OH)_3$, and $MgCO_3$. The $Al(OH)_3$ and $MgCO_3$ were dehydrated and decarbonated, respectively, at 1200 °C for 12 h. Fe_2O_3 was dried at 120 °C. The resulting oxides were then stored in a desiccator.

Stoichiometric oxide mixes were pressed into pellets and reacted in a vertical-tube furnace at a temperature of 1300 °C. For all samples, the atmosphere in the furnace had a CO_2/CO ratio of 333 ($\log f_{O_2} = -4.7$ at 1300 °C), corresponding to conditions of zero deviation from stoichiometry ($\delta = 0$) for the magnetite component in the solid solutions (Dieckmann, 1982). In order to obtain single-phase spinels for every composition, sample pellets were reacted for 8 h at 1300 °C after which they were ground, pressed into pellets, and again fired at the same temperature. Four such cycles proved sufficient to yield single-phase spinel solid solutions.

Once the desired compositions were prepared, the samples were crushed in a vibratory mill using alumina grinding medium and pressed into pellets at a pressure of 2.75×10^8 Pa in a cold isostatic press. The pellets were finally sintered at a temperature of 1300 °C for a period of 20 h in order to achieve high-density samples. Cell edges and densities (expressed as percentages of the theoretical densities for each composition) were determined after final sintering at 1300 °C (Table 1).

Thermopower and conductivity measurements were made using a four-point measurement technique in which four holes were drilled through rectangular bar specimens measuring approximately 1.5 × 1.5 × 15 mm with an ultrasonic drill. Each hole was threaded with a Pt_6Rh_{94}-$Pt_{30}Rh_{70}$ thermocouple. The threaded sample bar was then mounted on an eight-bore alumina thermocouple tube. The thermocouple leads were used to pull the fused thermocouple beads snugly against the sample in order to assure electrical contact between the thermocouple beads and the sample (Fig. 1). The sample was positioned off the hot-zone in a vertical, molybdenum disilicide–heated, alumina muffle furnace in such a position as to achieve an approximately 15 °C temperature gradient along the sample.

The thermopower-conductivity measurements were made at 100 °C intervals from 1400 °C down to 600 °C and then back to 1400 °C, following a grain-growth stabilization pre-anneal of 8 h at 1400 °C. Readings were recorded after thermal voltages were stable to ±1% over at least 30 min. At 600 °C and 700 °C, specimens were held for at least 12 h without significant changes in the readings. At all times, a gas mix with CO_2/CO ratio of 333 was passed over the sample at a flow rate of about 1 linear cm/s.

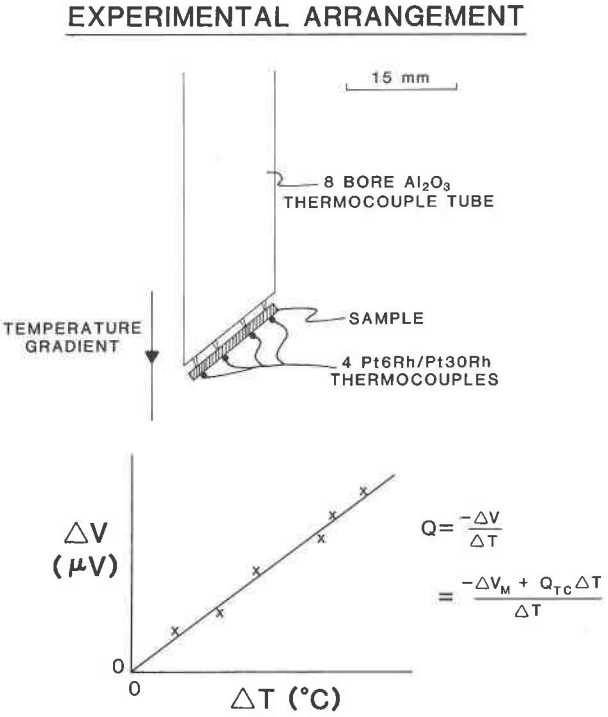

Fig. 1. Schematic illustration of experimental arrangement and typical ΔV vs. ΔT plot. Q_{TC} stands for the thermopower of the reference element of the thermocouple.

The four thermocouples and their common Pt_6Rh_{94} leads provided six ΔT values and six corresponding ΔE values. The slope of ΔE (emf) vs. ΔT when corrected for the thermopower of Pt_6Rh_{94}, is then the thermopower (in $\mu V \cdot K^{-1}$) (Fig. 1), i.e.,

$$Q = -\lim_{\Delta T \to 0}(\Delta V/\Delta T). \quad (8)$$

The temperature of the measurement was taken to be the average of the four thermocouples. The experimental uncertainty in each thermopower measurement may be evaluated from the correlation coefficient obtained from a linear regression through the six $\Delta T/\Delta E$ pairs as well as from the ΔT intercept at $\Delta E = 0$ (ΔT offset). In general, correlation coefficients were better than 0.995, whereas values of ΔT offset were smaller than ±0.3 °C.

Limits of the experimental uncertainty in the method used for measuring the thermopower may be evaluated from the maximum error in maximum ΔT, which is estimated at ±1 °C (Wu and Mason, 1981). Assuming a maximum temperature gradient of approximately 15 °C, this yields an uncertainty of about ±7%.

Following the thermopower measurement, small (milliampere) currents were passed in both directions between the outer thermocouples, and the voltage drop across the inner thermocouples was used to calculate the sample conductivity. This procedure allowed for the thermal voltage drop to be subtracted out of the measured emf's. Con-

TABLE 1. Sample characterization

		$Fe^{2+}Fe^{3+}_{2x}Al_{2-2x}O_4$			$Fe^{2+}_xMg_{1-x}Fe^{3+}_2O_4$		
	Fe_3O_4	$x = 0.25$	$x = 0.50$	$x = 0.75$	$x = 0.25$	$x = 0.50$	$x = 0.75$
FeO	30.92 (0.95)	38.66 (0.49)	36.00 (0.99)	33.41 (0.82)	9.89 (0.54)	17.09 (0.48)	24.22 (0.40)
Fe_2O_3*	68.71	20.35	38.22	54.42	74.88	72.94	69.81
MgO	—	—	—	—	13.78(0.07)	9.06(0.14)	4.43(0.09)
Al_2O_3	—	41.72(0.21)	26.70(0.09)	12.62(0.11)	1.02(0.07)	0.61(0.04)	0.98(0.05)
Total	99.63	100.73	100.92	100.45	99.57	99.70	99.44
No. analyses	3	8	4	5	7	6	8
$Fe^{2+}/(Fe^{2+} + Mg)$	1.0	1.0	1.0	1.0	0.28	0.51	0.75
$Fe^{3+}/(Fe^{3+} + Al)$	1.0	0.24	0.48	0.73	0.98	0.99	0.98
Cell edge (Å)**	8.3969(13)	8.1829(14)	8.2638(12)	8.3330(16)	8.3820(14)	8.3919(9)	8.3901(23)
Density†	96.9	88.7	93.5	95.0	90.1	91.8	92.0

Note: $\pm 1s$ values for each element are given in parentheses.
* Fe_2O_3 calculated from stoichiometry. Standard deviations are for total Fe.
** Numbers in parentheses are $\pm 1s$ for final decimal place.
† Percentage of theoretical density.

ductivity was then corrected for the percentage theoretical density. Experimental uncertainties in the conductivity measurements are difficult to evaluate because of the profound effect that microstructural features may have on the electrical conductivity of polycrystalline samples. The accuracy of the measurements was estimated by comparing the results obtained for magnetite with the results obtained by Dieckmann et al. (1983) on single-crystal magnetite. Measurements were found to be approximately 10% lower than the Dieckmann et al. results over the experimentally examined thermal range. The difference may be due to grain-boundary effects in the polycrystalline magnetite sample used in this study. In the present investigation, however, the precision of the measurements is of greater importance than the accuracy since the values are normalized relative to our polycrystalline magnetite values in Equation 6. Measurements taken going up and down temperature on the solid-solution samples were found to agree to within $\pm 10\%$ to $\pm 15\%$ of the mean values obtained from a linear regression through $\ln \sigma T$ vs. $1/T$ data points, and the precision of the conductivity measurements is therefore assumed to be of this order.

Following the electrical measurements, the specimen slabs as well as unused slabs of the same composition were mounted and polished for analysis by electron microprobe. In all cases, the used as well as unused material proved to be chemically homogeneous, single-phase spinel. Measured compositions with Fe^{3+} concentrations calculated from stoichiometry are reported in Table 1. No evidence was found for Fe depletion in the material surrounding the thermocouple holes, suggesting that possible Fe assimilation by the thermocouple beads had a negligible effect on spinel composition. Most samples show evidence for Al_2O_3 contamination due to the grinding step in the vibratory mill in the sample-preparation procedure. However, the contamination is sufficiently small (between 0.5 and 1%) to have a negligible effect on cation-distribution calculations.

RESULTS

Thermopower results for Fe_3O_4-$MgFe_2O_4$, Fe_3O_4-$FeAl_2O_4$, and Fe_3O_4-$MgAl_2O_4$ solid solutions are plotted in Figures 2A to 2C, respectively. Error bars on the data points correspond to a ± 1 °C uncertainty in maximum ΔT for every measurement. The data are reversible inasmuch as repeated heating and cooling cycles from 600 °C to 1400 °C and back again always produce the same results within experimental uncertainty. The magnetite data agree closely with the measurements of Wu and Mason (1981) on single-crystal material and are presented in each of Figures 2A, 2B, and 2C for comparison.

In the Fe_3O_4-$MgFe_2O_4$ solid solution, the absolute value of thermopower increases with magnetite dilution (Fig. 2A), whereas in the Fe_3O_4-$FeAl_2O_4$ system, it decreases in absolute value with magnetite dilution (Fig. 2B). The latter system also displays a decrease in the slope $[dQ/d(1/T)]$ with decreasing $|Q|$. For both solid solutions, the results are in excellent agreement with the measurements of Trestman-Matts et al. (1984) on the Fe_3O_4-$MgFe_2O_4$ system and those of Mason and Bowen (1981) on the Fe_3O_4-$FeAl_2O_4$ system, respectively. The relative changes in the absolute values of thermopower may be qualitatively interpreted from Equation 2. In the Fe_3O_4-$MgFe_2O_4$ system, there is an increase in the ratio $(Fe^{3+}/Fe^{2+})_{oct}$ because of the substitution of Mg for Fe^{2+}. The Fe_3O_4-$FeAl_2O_4$ system, on the other hand, has a decreasing ratio of $(Fe^{3+}/Fe^{2+})_{oct}$ due to the substitution of Al for Fe^{3+}.

Both of these substitutions are operative in the Fe_3O_4-$MgAl_2O_4$ solid solution, and the thermopower is thus expected—and observed—to remain relatively constant throughout the compositional range investigated (Fig. 2C). The slight decrease in the absolute value of thermopower, as well as the decrease in slope $[dQ/d(1/T)]$, indicates that the Al-Fe^{3+} substitution dominates the Mg-Fe^{2+} substitution in determining the behavior of the thermoelectric coefficient in this system.

The thermopower data have been fit to a polynomial of the form

$$Q = a + b(10^4/T) + c(10^4/T)^2, \quad (9)$$

where Q is in μV/K. The use of a second-degree term (c) is only required for three samples for which the statistical F-ratio yielded values that were above the 90% confidence level for a quadratic relative to a linear relationship (Be-

TABLE 1.—*Continued*

$Fe^{2+}_x Mg_{1-x} Fe^{3+}_{2x} Al_{2-2x} O_4$		
$x = 0.25$	$x = 0.50$	$x = 0.75$
11.35(0.62)	20.18(0.84)	25.66(0.76)
24.35	42.02	57.18
17.69(0.08)	10.37(0.10)	4.98(0.08)
45.19(0.22)	28.80(0.11)	13.13(0.12)
98.58	101.37	100.95
13	15	12
0.26	0.52	0.74
0.26	0.48	0.74
8.2268(7)	8.2834(7)	8.2400(9)
91.7	88.6	93.8

vington, 1969, p. 200). Values for the coefficients *a, b,* and *c* are reported in Table 2.

An unusual irreversible thermopower effect was observed in the $x = 0.25$ and 0.50 samples in the Fe_3O_4-$MgAl_2O_4$ solid solution after returning them to the furnace at 1400 °C. On cooling from 1400 °C to 1000 °C, these specimens exhibited larger absolute values of Q and larger $dQ/d(1/T)$ compared to the reversible measurements illustrated in Figure 2C. After reaching 1000 °C, however, repeated heating and cooling cycles of these specimens reproduced reversible results within experimental uncertainties (Fig. 2C). A final check on the reversibility of the thermopower measurements was conducted by taking measurements on an unused bar of the $x = 0.25$ material, starting at 600 °C, going up to 1400 °C and then down again to 600 °C. These values again agreed closely with the reversible measurements. A possible explanation for the irreversible behavior will be presented below.

Conductivity data for the Fe_3O_4-$MgFe_2O_4$, Fe_3O_4-$FeAl_2O_4$, and Fe_3O_4-$MgAl_2O_4$ solid solutions are presented in Figures 3A to 3C, respectively. The data follow linear relationships of the form

$$\ln \sigma T = A + B(10^4/T). \tag{10}$$

Values for the coefficients A and B are reported in Table 2. Error bars on the linear regression lines in Figures 3A to 3C correspond to uncertainties of ±10% to ±15% in the mean values calculated from Equation 10. No irreversibility was observed in the conductivity measurements of the Fe_3O_4-$MgAl_2O_4$ solid solution, whereas the measurements in the Fe_3O_4-$FeAl_2O_4$ systems are in good agreement with results obtained by Mason and Bowen (1981) at temperatures of 1500, 1600, and 1700 K.

Calculating $N_{(x_n)}$ from Equation 6 and solving for the amounts d and e in Equation 1 (see below) allows for a linear regression through $\ln \sigma T(d + e)/de$ vs. $1/T$ data points. This relationship is derived from Equation 4 when arranged in the form

$$\ln \frac{\sigma T(d+e)}{de} = \ln \frac{N e_0^2 a^2 \nu_0}{k} - \frac{E_H}{kT} = \ln A_0 - \frac{E_H}{kT}. \tag{11}$$

The resulting regression lines, therefore, have slopes of $-E_H/k$ and intercepts of $\ln A_0$.

Values of E_H for the solid-solution compositions are plotted in Figure 4. The activation energy for hopping shows a profound compositional dependence in the Fe_3O_4-$FeAl_2O_4$ and Fe_3O_4-$MgAl_2O_4$ systems, increasing from a value of 0.15 eV (magnetite) to about 0.40 eV for the $x = 0.25$ compositions (Fig. 4). The hopping energy in Fe_3O_4-$MgFe_2O_4$ solid solutions, on the other hand, changes only slightly, reaching a maximum value of about 0.20 eV for the $x = 0.25$ composition. The calculation of the error bars on the data points will be discussed below.

CATION DISTRIBUTIONS

Fe_3O_4-$MgFe_2O_4$ and Fe_3O_4-$FeAl_2O_4$ solid solutions

For mixtures containing x mole fractions of Fe_3O_4 and $(1 - x)$ mole fractions of $MgFe_2O_4$ and $FeAl_2O_4$, respectively, the thermopower-conductivity analysis enables calculation of the concentrations of Fe species on octahedral and tetrahedral sites through sets of equations based on compositional as well as mass- and charge-balance restrictions (Table 3).

At fixed mole fractions (x) of Fe_3O_4, it is necessary to measure two independent variables in Fe_3O_4-$MgFe_2O_4$ and Fe_3O_4-$FeAl_2O_4$ solid solutions in order to determine the unknowns in the structural formulae (Table 3). In this study, two such variables are given by the thermopower and conductivity measurements.

Remembering that $q = e/d = (Fe^{3+}/Fe^{2+})_{oct}$ and $N = (e + d) = (Fe^{3+} + Fe^{2+})_{oct}$, it may be shown that

$$d = N/(1 + q) \tag{12}$$

and

$$e = qN/(1 + q). \tag{13}$$

TABLE 2. Polynomial fit parameters for the thermopower and conductivity data sets

		$Fe^{2+}Fe^{3+}_{2x}Al_{2-2x}O_4$			$Fe^{2+}_x Mg_{1-x} Fe^{3+}_2 O_4$			$Fe^{2+}_x Mg_{1-x} Fe^{3+}_{2x} Al_{2-2x} O_4$		
	Fe_3O_4	$x = 0.25$	$x = 0.50$	$x = 0.75$	$x = 0.25$	$x = 0.50$	$x = 0.75$	$x = 0.25$	$x = 0.50$	$x = 0.75$
					Thermopower data					
a	−153.9	−59.8	−85.2	−119.2	−276.0	−213.7	−176.2	−81.7	−126.0	−145.2
b	6.3	6.3	3.5	4.7	8.2	7.5	6.9	1.2	5.3	8.8
c		−0.2	0.0	0.0	0.0	0.0	0.0	0.0	−0.1	−0.2
					Conductivity data					
A	14.506	12.830	13.209	13.457	12.713	13.205	13.488	10.397	12.467	13.241
B	−0.175	−0.455	−0.286	−0.267	−0.211	−0.206	−0.177	−0.448	−0.326	−0.253

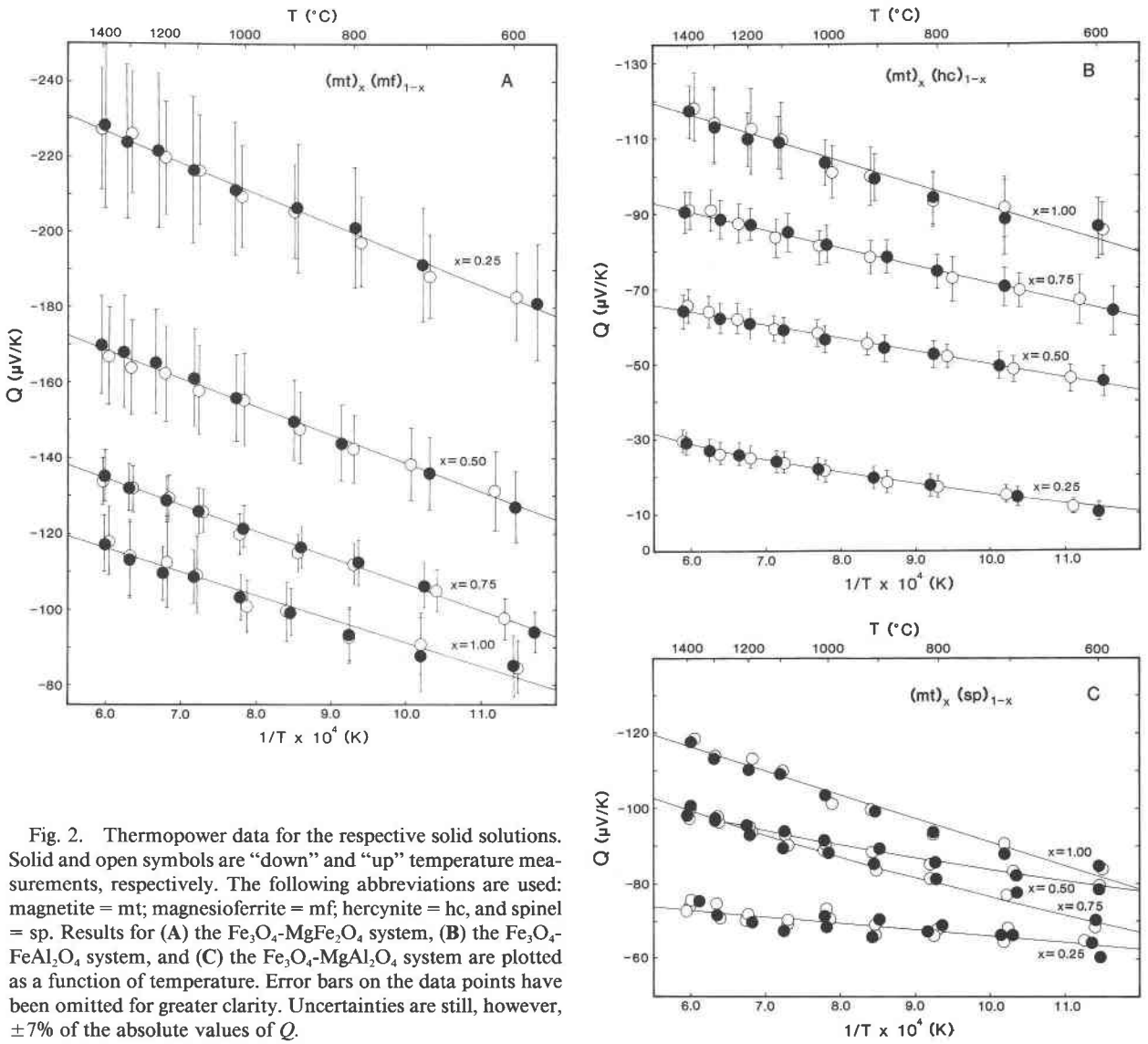

Fig. 2. Thermopower data for the respective solid solutions. Solid and open symbols are "down" and "up" temperature measurements, respectively. The following abbreviations are used: magnetite = mt; magnesioferrite = mf; hercynite = hc, and spinel = sp. Results for (**A**) the Fe_3O_4-$MgFe_2O_4$ system, (**B**) the Fe_3O_4-$FeAl_2O_4$ system, and (**C**) the Fe_3O_4-$MgAl_2O_4$ system are plotted as a function of temperature. Error bars on the data points have been omitted for greater clarity. Uncertainties are still, however, ±7% of the absolute values of Q.

These two measurements fully characterize the Fe^{2+}-Fe^{3+} distribution since they directly lead to the calculation of a and b through the relationships given in Table 3.

Uncertainties in the calculated cation distributions were estimated by considering the maximum uncertainties in the thermopower and conductivity measurements as outlined above. Maximum values for N were calculated by combining maximum and minimum values for $[c'(1 - c')]_{(x_1)}$ and $[c'(1 - c')]_{(x_n)}$, respectively, with the maximum conductivities for both magnetite and the solid-solution compositions in Equation 6. Minimum N values were calculated from the reverse procedure.

Following the O'Neill-Navrotsky (1983, 1984) model, ΔH_D values for Fe_3O_4-$MgFe_2O_4$ (mt-mf) and Fe_3O_4-$FeAl_2O_4$ (mt-hc) solid solutions are given by Equations 14 and 15, respectively:

$$\Delta H_D^{\text{mt-mf}} = \text{Mg}_{\text{oct}}[\alpha_{\text{Mg-Fe}^{3+}} + \beta_{\text{Mg-Fe}^{3+}}(\text{Mg}_{\text{oct}} + \text{Fe}^{2+}_{\text{oct}})] + \text{Fe}^{2+}_{\text{oct}}[\alpha_{\text{Fe}^{2+}\text{-Fe}^{3+}} + \beta_{\text{Fe}^{2+}\text{-Fe}^{3+}}(\text{Mg}_{\text{oct}} + \text{Fe}^{2+}_{\text{oct}})] \quad (14)$$

and

$$\Delta H_D^{\text{mt-hc}} = \text{Fe}^{3+}_{\text{tet}}[\alpha_{\text{Fe}^{2+}\text{-Fe}^{3+}} + \beta_{\text{Fe}^{2+}\text{-Fe}^{3+}}(\text{Fe}^{3+}_{\text{tet}} + \text{Al}_{\text{tet}})] + \text{Al}_{\text{tet}}[\alpha_{\text{Fe}^{2+}\text{-Al}} + \beta_{\text{Fe}^{2+}\text{-Al}}(\text{Fe}^{3+}_{\text{tet}} + \text{Al}_{\text{tet}})], \quad (15)$$

where α and β are energy parameters introduced by O'Neill and Navrotsky (1983). Theoretical cation distributions may be calculated as follows, given the α and β values of Table 4. For the $Fe_3O_4MgFe_2O_4$ join we have

$$-RT \ln \frac{\text{Fe}^{2+}_{\text{oct}}\text{Fe}^{3+}_{\text{tet}}}{\text{Fe}^{2+}_{\text{tet}}\text{Fe}^{3+}_{\text{oct}}} = \alpha_{\text{Fe}^{2+}\text{-Fe}^{3+}} + 2\beta_{\text{Fe}^{2+}\text{-Fe}^{3+}}\text{Fe}^{2+}_{\text{oct}} + (\beta_{\text{Fe}^{2+}\text{-Fe}^{3+}} + \beta_{\text{Mg-Fe}^{3+}})\text{Mg}_{\text{oct}} \quad (16)$$

and

$$-RT \ln \frac{\text{Mg}_{\text{oct}}\text{Fe}^{3+}_{\text{tet}}}{\text{Mg}_{\text{tet}}\text{Fe}^{3+}_{\text{oct}}} = \alpha_{\text{Mg-Fe}^{3+}} + 2\beta_{\text{Mg-Fe}^{3+}}\text{Mg}_{\text{oct}} + (\beta_{\text{Fe}^{2+}\text{-Fe}^{3+}} + \beta_{\text{Mg-Fe}^{3+}})\text{Fe}^{2+}_{\text{oct}}. \quad (17)$$

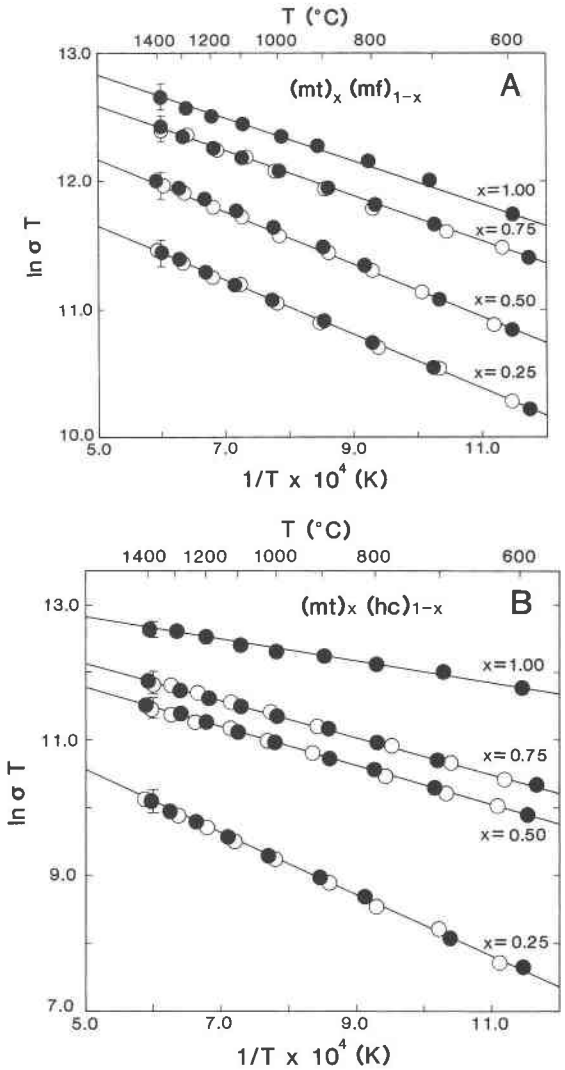

Fig. 3. Conductivity data for the respective solid solutions. Solid and open symbols are "down" and "up" temperature measurements, respectively. Results for (**A**) the Fe_3O_4-$MgFe_2O_4$ system, (**B**) the Fe_3O_4-$FeAl_2O_4$ system, and (**C**) the Fe_3O_4-$MgAl_2O_4$ system are plotted as a function of temperature.

TABLE 3. Mass- and charge-balance constraints and compositional relations in the Fe_3O_4-$FeAl_2O_4$, Fe_3O_4-$MgFe_2O_4$, and Fe_3O_4-$MgAl_2O_4$ solid solutions

System:	$(Fe_3O_4)_x(FeAl_2O_4)_{(1-x)}$
Structural formula:	$Fe_a^{2+}Fe_b^{3+}Al_n(Fe_d^{2+}Fe_e^{3+}Al_p)_2O_4$
	$a + b + n = 1$
	$d + e + p = 2$
	$2(a + d) + 3(b + e + n + p) = 8$
	$b + e = 2x$
System:	$(Fe_3O_4)_x(MgFe_2O_4)_{(1-x)}$
Structural formula:	$Fe_a^{2+}Fe_b^{3+}Mg_m(Fe_d^{2+}Fe_e^{3+}Mg_o)_2O_4$
	$a + b + m = 1$
	$d + e + o = 2$
	$2(a + d + m + o) + 3(b + e) = 8$
	$a + d = x$
System:	$(Fe_3O_4)_x(MgAl_2O_4)_{(1-x)}$
Structural formula:	$Fe_a^{2+}Fe_b^{3+}Mg_mAl_n(Fe_d^{2+}Fe_e^{3+}Mg_oAl_p)_2O_4$
	$a + b + m + n = 1$
	$d + e + o + p = 2$
	$2(a + d + m + o) + 3(b + e + n + p) = 8$
	$a + b + d + e = 3x$
	$b + e = 2(a + d)$

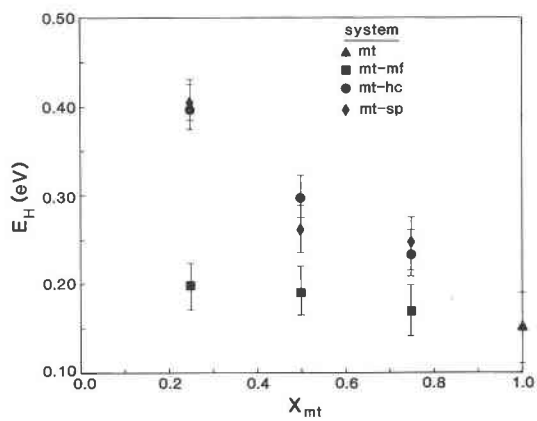

Fig. 4. Activation energies of hopping for the Fe_3O_4-$MgFe_2O_4$, Fe_3O_4-$FeAl_2O_4$, and Fe_3O_4-$MgAl_2O_4$ solid solutions as a function of sample composition.

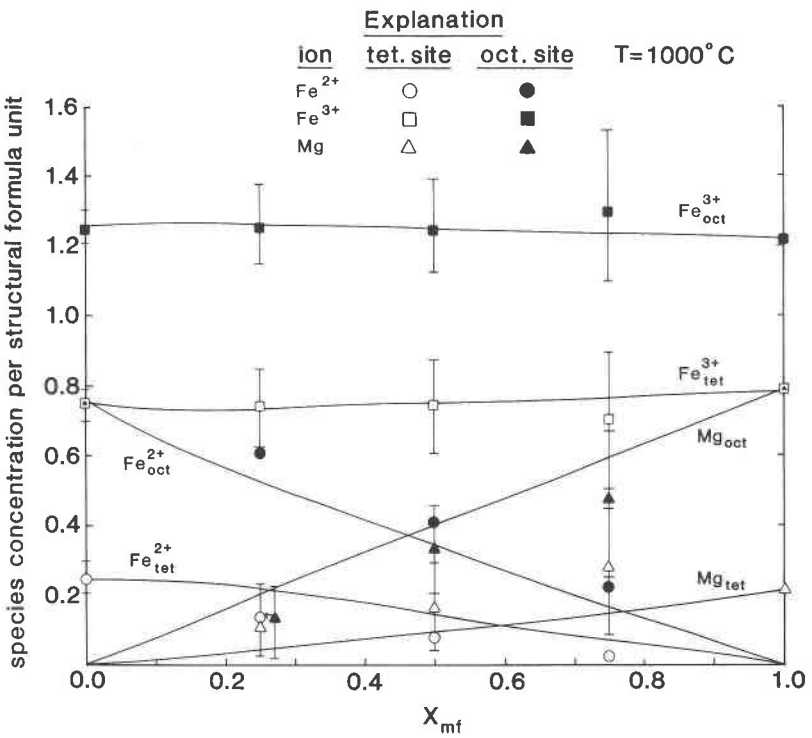

Fig. 5. Calculated intersite cation distributions compared to the measured values at 1000 °C in Fe_3O_4-$MgFe_2O_4$ solid solutions.

For Fe_3O_4–$FeAl_2O_4$ solid solutions, the conditions of equilibrium are

$$-RT \ln \frac{Fe^{2+}_{oct}Al_{tet}}{Fe^{2+}_{tet}Al_{oct}} = \alpha_{Fe^{2+}\text{-}Al} + 2\beta_{Fe^{2+}\text{-}Al}Al_{tet} + (\beta_{Fe^{2+}\text{-}Al} + \beta_{Fe^{2+}\text{-}Fe^{3+}})Fe^{3+}_{tet} \quad (18)$$

and

$$-RT \ln \frac{Fe^{2+}_{oct}Fe^{3+}_{tet}}{Fe^{2+}_{tet}Fe^{3+}_{oct}} = \alpha_{Fe^{2+}\text{-}Fe^{3+}} + 2\beta_{Fe^{2+}\text{-}Fe^{3+}}Fe^{3+}_{tet} + (\beta_{Fe^{2+}\text{-}Al} + \beta_{Fe^{2+}\text{-}Fe^{3+}})Al_{tet}. \quad (19)$$

TABLE 4. Internally consistent parameter set used for the calculation of intersite cation distributions

Parameter	Value (kJ/mol)
$\alpha_{Fe^{2+}\text{-}Fe^{3+}}$	33.75
$\beta_{Fe^{2+}\text{-}Fe^{3+}}$	−26.36
$\alpha_{Fe^{2+}\text{-}Al}$	50.98
$\beta_{Fe^{2+}\text{-}Al}$	−32.85
$\alpha_{Mg\text{-}Fe^{3+}}$	20.96
$\beta_{Mg\text{-}Fe^{3+}}$	−19.13
$\alpha_{Mg\text{-}Al}$	38.19
$\beta_{Mg\text{-}Al}$	−25.62
$\alpha_{Fe^{2+}\text{-}Mg}$	−12.79
$\beta_{Fe^{2+}\text{-}Mg}$	7.23

The nonlinear simultaneous equations were solved using the Newton-Raphson method (e.g., Gerald and Wheatley, 1984, p. 133–159) and the results for the Fe_3O_4-$MgFe_2O_4$ and Fe_3O_4-$FeAl_2O_4$ solid solutions, calculated at 1000 °C are presented as the solid curves in Figures 5 and 6, respectively. The solid lines are curves based on Equations 16 to 19 with the best-fit values of α and β given in Table 4. It may be seen from Figure 5 that the model works well for Fe_3O_4-$MgFe_2O_4$ spinels, but is less satisfactory for Fe_3O_4-$FeAl_2O_4$ solid solutions (Fig. 6). This may be ascribed to the different degrees of disorder of the end-members magnetite, hercynite, and magnesioferrite and of the solid solutions between them.

The O'Neill-Navrotsky model requires that each of the cation-distribution equilibria (Eqs. 16 to 19) be a linear function of the degree of inversion ($Al_{tet} + Fe^{3+}_{tet}$) and that α and β for each equilibrium be constant. It works well for Fe_3O_4-$MgFe_2O_4$ because both end-members in the solid solution have similar degrees of disorder at any particular temperature. Thus the partition coefficients

$$K_{Cd}^{Mg-Fe^{3+}} = (Mg_{oct}Fe^{3+}_{tet})/(Mg_{tet}Fe^{3+}_{oct})$$

and

$$K_{Cd}^{Fe^{2+}-Fe^{3+}} = (Fe^{3+}_{tet}Fe^{2+}_{oct})/(Fe^{3+}_{oct}Fe^{2+}_{tet})$$

are virtually independent of composition and the degree of inversion. The β term, therefore, does not change across the solid-solution series. In fact, dependence on the degree of inversion is so small that both $-RT \ln K_{Cd}^{Fe^{2+}\text{-}Fe^{3+}}$ and

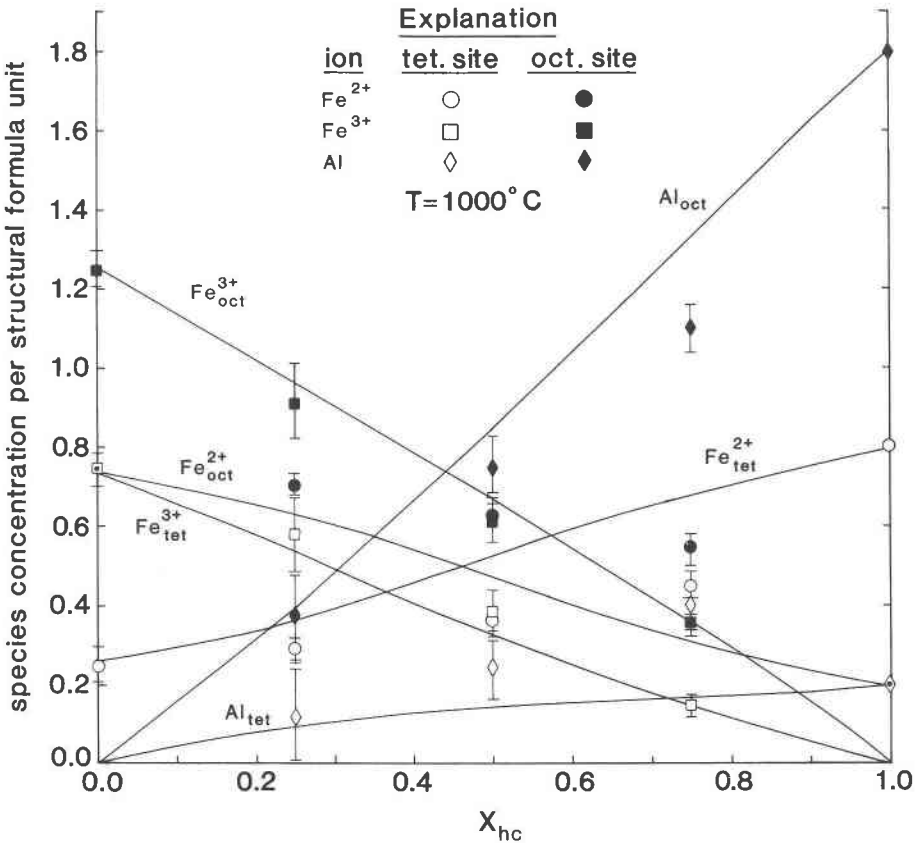

Fig. 6. Calculated intersite cation distributions compared to the measured values at 1000 °C in Fe_3O_4-$FeAl_2O_4$ solid solutions.

$-RT \ln K_{Cd}^{Mg\text{-}Fe^{3+}}$ could be modeled as constant as originally proposed by Navrotsky and Kleppa (1967). In the Fe_3O_4-$FeAl_2O_4$ system, on the other hand, Fe_3O_4 is always substantially more inverse than $FeAl_2O_4$, and for this solid solution, both α and β terms are very important. Our observed partitioning behavior suggests that $-RT \ln K_{Cd}^{Fe^{2+}\text{-}Fe^{3+}}$ is, as predicted, a function of the degree of inversion in the system (Fig. 7) and that the α and β parameters for this exchange equilibrium agree well with those for pure magnetite. Similarly, the partitioning behavior of $-RT \ln K_{Cd}^{Fe^{2+}\text{-}Al}$ is also a linear function of the degree of inversion over the examined compositional range (Fig. 8), but the α and β parameters in this case do not agree with those for pure hercynite. Moreover, $\alpha_{Fe^{2+}\text{-}Al}$ and $\beta_{Fe^{2+}\text{-}Al}$ need to be composition dependent to describe the partitioning behavior.

Fe_3O_4-$MgAl_2O_4$ solid solutions

In this system, measurements of three of the four cation-distribution equilibria (Eqs. 16 to 19) are required to fully characterize the distributions of cations between octahedral and tetrahedral sites. Given measurements of the Fe^{2+}-Fe^{3+} distribution, it is necessary to fix the distribution of one other cation in order to derive all site occupancies. If we assume that the O'Neill-Navrotsky model works for the Fe_3O_4-$MgAl_2O_4$ join, then the concentration of tetrahedral Al is given by (extended form of Eq. 19)

$$\alpha_{Fe^{2+}\text{-}Fe^{3+}} + Al_{tet}(\beta_{Fe^{2+}\text{-}Fe^{3+}} + \beta_{Fe^{2+}\text{-}Al}) + 2Fe_{tet}^{3+}\beta_{Fe^{2+}\text{-}Fe^{3+}} + (\beta_{Fe^{2+}\text{-}Fe^{3+}} + \beta_{Fe^{2+}\text{-}Mg})Mg_{oct} = -RT \ln \frac{Fe_{tet}^{3+}Fe_{oct}^{2+}}{Fe_{tet}^{2+}Fe_{oct}^{3+}}. \quad (20)$$

Using the measured Fe^{2+}-Fe^{3+} distributions, Equation 20 is readily solved for Al_{tet}. Then, with the site and mass-balance constraints of Table 3, all cation occupancies are fixed. The results are shown in Figure 9 together with calculated curves obtained from the O'Neill-Navrotsky treatment. The latter were derived by solving Equation 20 together with the analogous expansions of Equation 18 and a Mg-Fe^{2+} exchange equilibrium obtained from Equations 16 and 17,

$$\alpha_{Fe^{2+}\text{-}Al} + Fe_{tet}^{3+}(\beta_{Fe^{2+}\text{-}Fe^{3+}} + \beta_{Fe^{2+}\text{-}Al}) + 2Al_{tet}\beta_{Fe^{2+}\text{-}Al} + (\beta_{Fe^{2+}\text{-}Al} + \beta_{Fe^{2+}\text{-}Mg})Mg_{oct} = -RT \ln \frac{Al_{tet}Fe_{oct}^{2+}}{Al_{oct}Fe_{tet}^{2+}} \quad (21)$$

$$\alpha_{Fe^{2+}\text{-}Mg} + Fe_{tet}^{3+}(\beta_{Fe^{2+}\text{-}Fe^{3+}} + \beta_{Fe^{2+}\text{-}Mg}) + Al_{tet}(\beta_{Fe^{2+}\text{-}Al} + \beta_{Fe^{2+}\text{-}Mg}) + 2Mg_{oct}\beta_{Fe^{2+}\text{-}Mg} = -RT \frac{Mg_{oct}Fe_{tet}^{2+}}{Mg_{tet}Fe_{oct}^{2+}}, \quad (22)$$

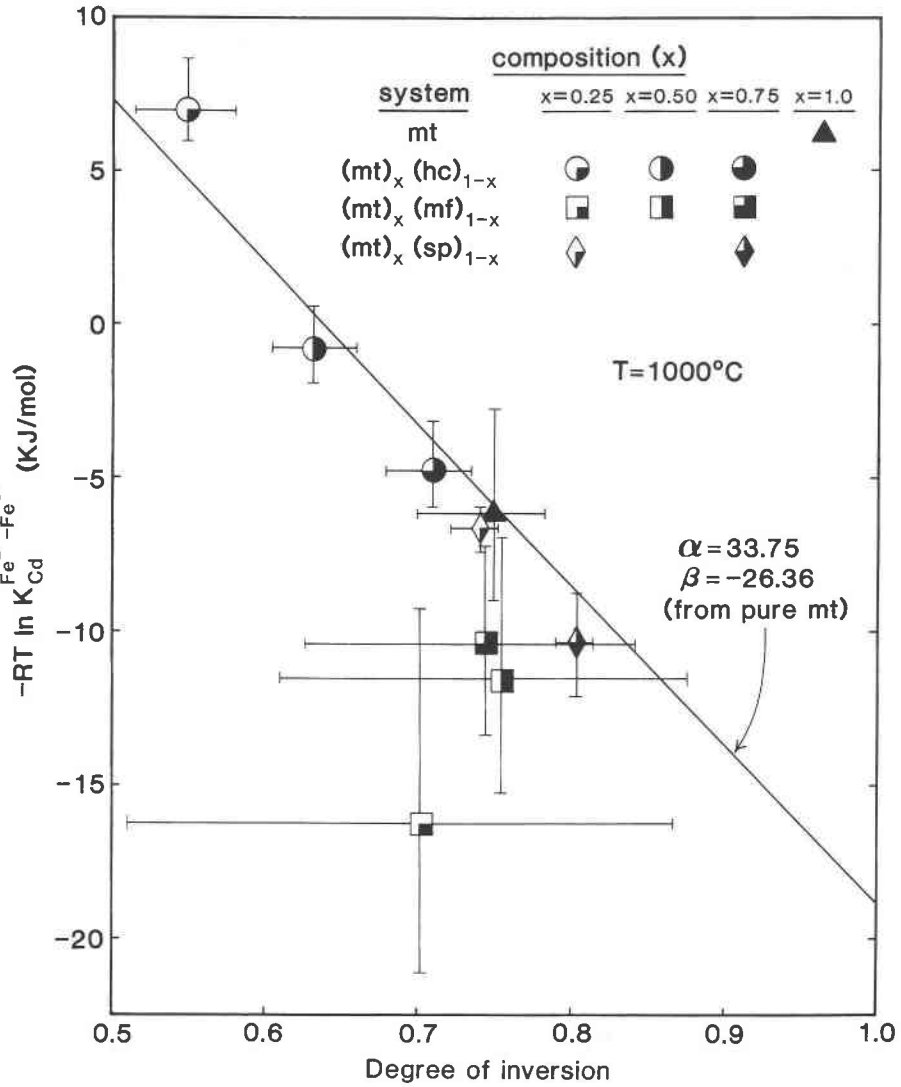

Fig. 7. Intersite distributions of Fe^{2+} and Fe^{3+} as a function of tetrahedral trivalent ions at 1000 °C for the Fe_3O_4-$MgFe_2O_4$, Fe_3O_4-$FeAl_2O_4$, and Fe_3O_4-$MgAl_2O_4$ solid solutions. Solid line calculated from the $\alpha_{Fe^{2+}\text{-}Fe^{3+}}$ and $\beta_{Fe^{2+}\text{-}Fe^{3+}}$ values for pure magnetite agrees well with the observed partitioning data. The $x = 0.50$ data point for the Fe_3O_4-$MgAl_2O_4$ system is not shown for clarity. It plots between the magnetite and 25% magnetite–75% spinel data points.

and two site and three mass-balance equations (Table 3 and Mattioli and Wood, 1988).

The α and β values used for the solution of these eight equations (Table 4) are our best-fit values of Table 5 that have been forced to be internally consistent, i.e.,

$$\alpha_{Fe^{2+}\text{-}Fe^{3+}} + \alpha_{Mg\text{-}Al} = \alpha_{Fe^{2+}\text{-}Al} + \alpha_{Mg\text{-}Fe^{3+}}$$
$$\beta_{Fe^{2+}\text{-}Fe^{3+}} + \beta_{Mg\text{-}Al} = \beta_{Fe^{2+}\text{-}Al} + \beta_{Mg\text{-}Fe^{3+}}. \quad (23)$$

As can be seen from Figure 9, the observed distributions, which have the assumption that the Fe^{2+}-Fe^{3+} distribution obeys the O'Neill-Navrotsky model, are in good agreement with the model values in which all four cations are forced to obey the model. Although the argument has an element of circularity to it, it is clear that the Fe^{2+}-Fe^{3+} cation-partitioning data are broadly consistent with the simple model.

Discussion

In the simplest type of model (Navrotsky and Kleppa, 1967), the logarithm of any particular intersite distribution coefficient ($-RT \ln K_{Cd}$) is a constant independent of the degree of inversion. The O'Neill-Navrotsky model (Eqs. 16–19), on the other hand, predicts a linear dependence of $-RT \ln K_{Cd}$ on the tetrahedral occupancy of trivalent ions. Figure 7 shows the 1000 °C data that we have collected for the joins Fe_3O_4-$MgFe_2O_4$, Fe_3O_4-$FeAl_2O_4$, and Fe_3O_4-$MgAl_2O_4$ and for pure magnetite plotted so as to illustrate the dependence of $-RT \ln K_{Cd}^{Fe^{2+}\text{-}Fe^{3+}}$ on the degree of inversion. It may be seen that

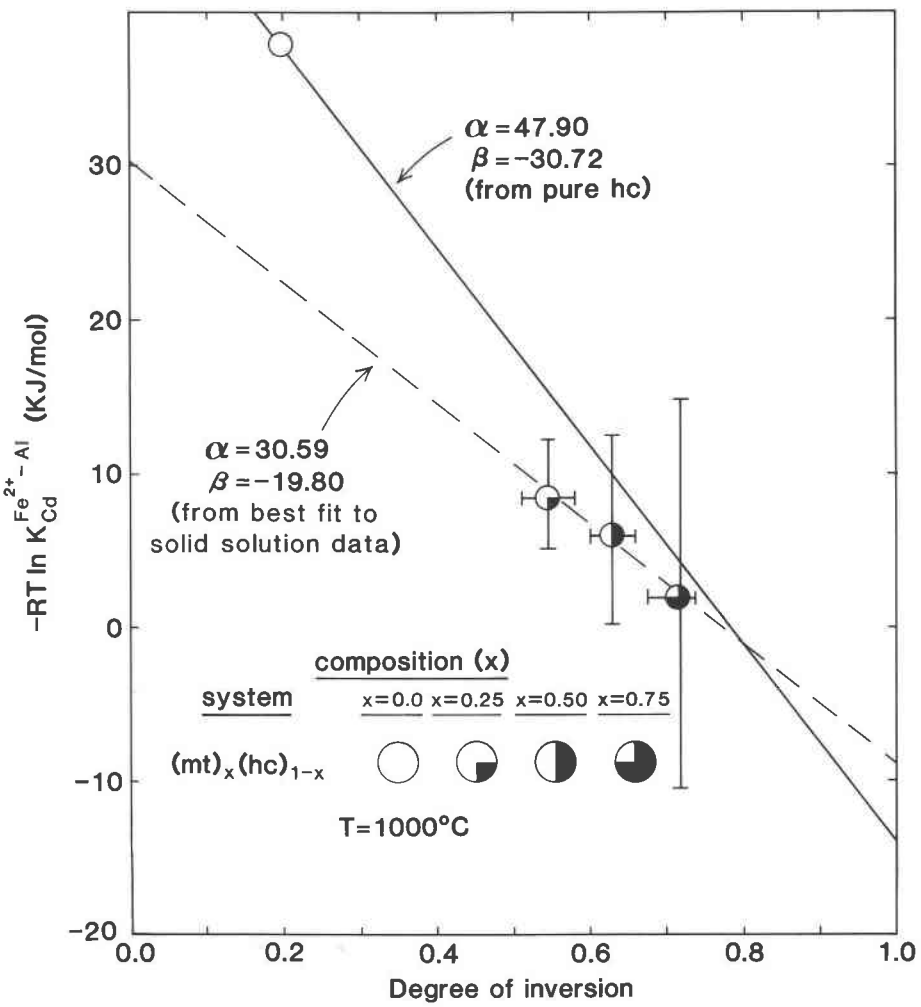

Fig. 8. Intersite distributions of Fe^{2+} and Al as a function of total tetrahedral trivalent ion occupancy in Fe_3O_4-$FeAl_2O_4$ solid solutions. Best-fit α and β parameters to the solid-solution data are significantly different from those calculated for pure hercynite.

the data for Fe_3O_4-$MgFe_2O_4$, Fe_3O_4-$FeAl_2O_4$, and Fe_3O_4-$MgAl_2O_4$ fit quite well to the O'Neill-Navrotsky model using the $\alpha_{Fe^{2+}\text{-}Fe^{3+}}$ and $\beta_{Fe^{2+}\text{-}Fe^{3+}}$ values derived from pure magnetite. The fit obtained for Fe_3O_4-$MgFe_2O_4$ does not provide a stringent test of the model, however, since the data also fit reasonably well to the constant $-RT \ln K_{Cd}$ (Navrotsky-Kleppa) model. In Fe_3O_4-$FeAl_2O_4$ (Fig. 8), $-RT \ln K_{Cd}^{Fe^{2+}\text{-}Al}$ is approximately linearly dependent on total trivalent ion occupancy, exhibiting qualitative agreement with the O'Neill-Navrotsky model. The Fe^{2+}-Al distribution data for this join are not, however, reproduced by the $\alpha_{Fe^{2+}\text{-}Al}$ and $\beta_{Fe^{2+}\text{-}Al}$ values for pure hercynite. Therefore the O'Neill-Navrotsky model does not fit unless provision is made for compositional dependence of the $\alpha_{Fe^{2+}\text{-}Al}$ and $\beta_{Fe^{2+}\text{-}Al}$ parameters. A detailed discussion of the implications of these observations for predicting the macroscopic thermodynamic properties of spinels will be presented in a future paper.

Table 5. α and β parameters obtained from least-squares fits through cation-distribution data for pure magnetite, hercynite, magnesioferrite, and spinel

Parameter	Value (kJ/mol)	Source
$\alpha_{Fe^{2+}\text{-}Fe^{3+}}$	33.75 ± 1.92	This study
$\beta_{Fe^{2+}\text{-}Fe^{3+}}$	−26.36 ± 1.34	
$\alpha_{Fe^{2+}\text{-}Al}$	47.90 ± 3.6	(see below)*
$\beta_{Fe^{2+}\text{-}Al}$	−30.72 ± 2.01	
$\alpha_{Mg\text{-}Fe^{3+}}$	17.88 ± 3.07	(see below)†
$\beta_{Mg\text{-}Fe^{3+}}$	−17.00 ± 1.84	
$\alpha_{Mg\text{-}Al}$	38.19 ± 0.31	Wood et al. (1986)
$\beta_{Mg\text{-}Al}$	−25.62 ± 0.54	

* Bohlen et al. (1986); Hill (1984); Chassagneux and Rousset (1976); Yagnik and Mathur (1968).

† Pauthenet and Bochirol (1951); Kriessman and Harrison (1956); Epstein and Frackiewicz (1958); Mozzi and Paladino (1963); Blasse (1964); Tellier (1967).

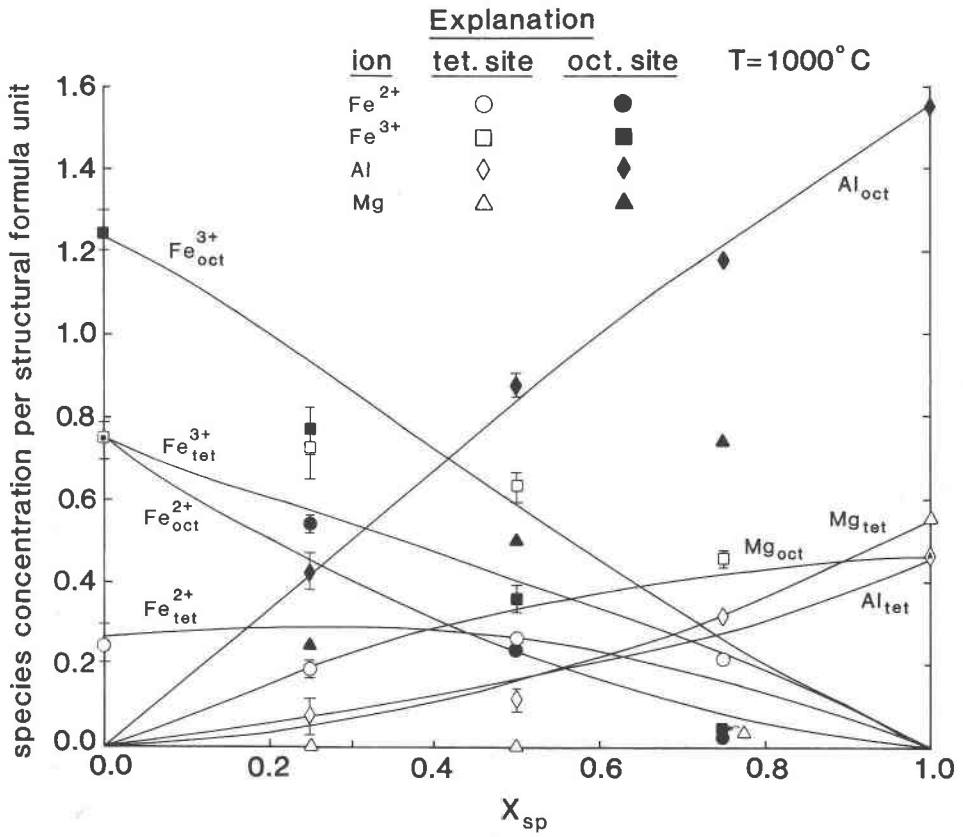

Fig. 9. Calculated intersite cation distributions compared to the measured values at 1000 °C in Fe_3O_4-$MgAl_2O_4$ solid solutions.

As noted earlier, irreversible thermopower results were obtained in some experiments at high mole fractions of $MgAl_2O_4$. A possible explanation for this behavior is that it is due to disequilibrium order-disorder phenomena. In their NMR study of order-disorder relations in $MgAl_2O_4$, Wood et al. (1986) found that the macroscopically determined entropy of Mg-Al disorder is much lower than would be predicted from the octahedral-tetrahedral cation distribution. They then concluded that there was substantial short-range order in the spinel structure that acts to lower the configurational entropy. Similar short-range ordering has also been proposed for $MgFe_2O_4$ spinel by Kroger (1964 and references therein). In this study it was found that the differences between reversible and irreversible thermopower measurements increased with increasing $MgAl_2O_4$ content of the spinel. It is therefore possible that the irreversible thermopower measurements are due to the same type of short-range ordering phenomenon that has already been discussed with respect to $MgAl_2O_4$ (Wood et al., 1986).

Samples sintered at 1300 °C and then quenched should be relatively disordered. We suggest that if such samples are returned to the furnace at 1400 °C they remain relatively disordered with higher Fe^{3+}/Fe^{2+} ratios on the octahedral site than the reversible material. As they are cooled, the free-energy difference between disordered and ordered states progressively increases until at about 900 °C the samples undergo rapid short-range ordering. Thereafter, repeated heating and cooling cycles produced reversible thermopower results corresponding to the equilibrium extent of short-range order. The only unusual feature of our observations is that disequilibrium is apparently maintained for long periods (up to approximately 48 h) at very high temperatures. This must be due either to an extremely small free-energy difference between ordered and disordered states at high temperatures or to a kinetic barrier to ordering. During the cooling cycle from 1400 °C down to 900 °C, the sample undergoes appreciable long-range ordering of Mg and Al as well as Fe^{2+} and Fe^{3+}, and it is possible that the highly (long-range) disordered Mg-Al distribution at high temperature initially inhibits clustering of Fe^{2+} and Fe^{3+}. If this is the case, the Fe^{2+} and Fe^{3+} will reorder rapidly once a critical value of the inversion parameter for $MgAl_2O_4$ is reached.

It is unclear at this stage how the cation-distribution analysis might be affected by short-range ordering. The lack of a quantitative model precludes the explicit treatment of short-range order in the calculation of cation distributions.

Conclusions

The thermopower-conductivity technique has been successfully employed to examine intersite cation distributions in Fe_3O_4-$MgFe_2O_4$, Fe_3O_4-$FeAl_2O_4$, and Fe_3O_4-

$MgAl_2O_4$ solid solutions. The measurements indicate that Fe^{2+}-Fe^{3+} distributions become increasingly inverse in Fe_3O_4-$MgFe_2O_4$ solid solutions with magnetite dilution, whereas they become more normal in the Fe_3O_4-$FeAl_2O_4$ system as magnetite content decreases. In Fe_3O_4-$MgAl_2O_4$ solid solutions, the Fe^{2+}-Fe^{3+} distribution is similar to that of magnetite. In addition there are strong enrichments of both Fe^{2+} and Fe^{3+} on the tetrahedral site in the dilute magnetite part of the solid-solution series. In-situ measurements of cation distributions provide a necessary bridge between macroscopic thermodynamic measurements of free energy, entropy, etc. and the hypothetical ordering schemes generally used for spinel end-members. The latter may only be used to extrapolate thermodynamic properties if they can be confirmed by direct measurement at high temperature. In this study, we have found that the O'Neill-Navrotsky (1983, 1984) model of cation distribution provides a good approximation of the properties of Fe_3O_4-$MgFe_2^{3+}O_4$ spinels, but it is less successful in predicting cation distributions in Fe_3O_4-$FeAl_2O_4$ solid solutions. In Fe_3O_4-$MgAl_2O_4$ spinels, the Fe^{2+}-Fe^{3+} partitioning data are broadly consistent with calculated values assuming that all four cations in the solid solution behave according to the O'Neill-Navrotsky model. From this study, it is evident that a more accurate representation of cation distributions in complex spinel solid solutions may be achieved by also considering the compositional dependencies of the various distribution coefficients. Such a model, using a second-degree Taylor expansion of the vibrational part of the Gibbs free energy of a solid solution in terms of both compositional and order parameters will be presented in a forthcoming paper.

Acknowledgments

This research was made possible in part by financial support from the Council for Mineral Technology (MINTEK) to J.N. Support by NSF Grant EAR-8416793 to B.J.W. is also acknowledged. J.N. would like to thank George Hellfrich for valuable assistance in writing a computer program for the solution of simultaneous nonlinear equations. We also acknowledge constructive reviews of the manuscript by A. Navrotsky and R. O. Sack.

References cited

Bevington, P.R. (1969) Data reduction and error analysis for the physical sciences, 336 p. McGraw-Hill, New York.

Blasse, G. (1964) Crystal chemistry and some magnetic properties of mixed metal oxides with spinel structure, 139 p. Philips Research reports, Supplement no. 3, Mahwah, New Jersey.

Bohlen, S.R., Dollase, W.A., and Wall, V.J. (1986) Calibration and application of spinel equilibria in the system FeO-Al_2O_3-SiO_2. Journal of Petrology, 27, 1143–1156.

Buddington, A.F., and Lindsley, D.H. (1964) Iron-titanium oxide minerals and their synthetic equivalents. Journal of Petrology, 5, 310–357.

Chassagneux, F., and Rousset, A. (1976) Preparation and structural study of $FeAl_{2-2z}Cr_{2z}O_4$ spinel. Journal of Solid State Chemistry, 16, 161–166.

Dieckmann, R. (1982) Defects and cation diffusion in magnetite (IV): Nonstoichiometry and point defect structure of magnetite ($Fe_{3-\delta}O_4$). Berichte Bunsengesellschaft Physikalische Chemie, 86, 112–118.

Dieckmann, R., Witt, C.A., and Mason, T.O.M. (1983) Defects and cation diffusion in magnetite (V): Electrical conduction, cation distribution and point defects in magnetite ($Fe_{3-\delta}O_4$). Berichte Bunsengesellschaft Physikalische Chemie, 87, 495–503.

Epstein, D.J., and Frackiewicz, B. (1958) Some properties of quenched magnesium ferrites. Journal of Applied Physics, 29, 376–377.

Gasparik, T., and Newton, R.C. (1984) The reversed alumina contents of orthopyroxene in equilibrium with spinel and forsterite in the system MgO-Al_2O_3-SiO_2. Contributions to Mineralogy and Petrology, 85, 186–196.

Gerald, C.F., and Wheatley, P.O. (1984) Applied numerical analysis, 579 p. Addison-Wesley, Reading, Massachusetts.

Hill, R.J. (1984) X-ray powder diffraction profile refinement of synthetic hercynite. American Mineralogist, 69, 937–942.

Kriessman, C.J., and Harrison, S.E. (1956) Cation distributions in ferrospinels. Magnesium-manganese ferrites. Physical Review, 103, 857–860.

Kroger, F.A. (1964) The chemistry of imperfect crystals, 1039 p. North-Holland, Amsterdam.

Kuendig, W., and Hargrove, R.S. (1969) Electron hopping in magnetite. Solid State Communications, 7, 223–227.

Mason, T.O. (1985) High-temperature cation distributions in Fe_3O_4-$FeAl_2O_4$. American Ceramic Society Journal, 68, C74–75.

——— (1987) Cation intersite distributions in iron-bearing minerals via electrical conductivity/seebeck effect. Physics and Chemistry of Minerals, 14, 156–162.

Mason, T.O., and Bowen, H.K. (1981) Electronic conduction and thermopower of magnetite and iron-aluminate spinels. American Ceramic Society Journal, 64, 237–242.

Mattioli, G.S., and Wood, B.J. (1988) Magnetite activities across the $MgAl_2O_4$-Fe_3O_4 spinel join, with application to the thermobarometric estimates of upper mantle oxygen fugacity. Contributions to Mineralogy and Petrology, 98, 148–162.

Mozzi, R.L., and Paladino, A.E. (1963) Cation distributions in nonstoichiometric magnesium ferrite. Journal of Chemical Physics, 39, 435–439.

Navrotsky, A., and Kleppa, O.J. (1967) Thermodynamics of formation of simple spinels. Journal of Inorganic and Nuclear Chemistry, 30, 479–498.

O'Neill, H.St.C., and Navrotsky, A. (1983) Simple spinels: Crystallographic parameters, cation radii, lattice energies, and cation distribution. American Mineralogist, 68, 181–194.

——— (1984) Cation distribution and thermodynamic properties of binary spinel solid solutions. American Mineralogist, 69, 733–753.

Pauthenet, R., and Bochirol, L. (1951) Spontaneous magnetization of ferrites. Journal de Physique et de Radium, 12, 249–251 (in French).

Sack, R. O. (1982) Spinels as petrogenetic indicators: Activity-composition relations at low pressure. Contributions to Mineralogy and Petrology, 71, 169–186.

Tellier, J-C. (1967) On the substitution of Fe^{3+} in magnesium ferrite by trivalent, tetravalent and pentavalent cations. Revue de Chimie Minérale, 4, 325–365 (in French).

Trestman-Matts, A., Dorris, S.E., Kumarakrishnan, S., and Mason, T.O. (1983) Thermoelectric determination of cation distributions in Fe_3O_4-Fe_2TiO_4. American Ceramic Society Journal, 66, 829–834.

Trestman-Matts, A., Dorris, S.E., and Mason, T.O. (1984) Thermoelectric determination of cation distributions in Fe_3O_4-$MgFe_2O_4$. American Ceramic Society Journal, 67, 69–73.

Tuller, H.L., and Nowick, A.S. (1977) Small polaron transport in reduced CeO_2 single crystals. Journal of Physical Chemistry of Solids, 38, 859–867.

Wood, B.J., Kirkpatrick, R.J., and Montez, B. (1986) Order-disorder phenomena in $MgAl_2O_4$ spinel. American Mineralogist, 71, 999–1006.

Wu, C.C., and Mason, T.O. (1981) Thermopower measurement of cation distribution in magnetite. American Ceramic Society Journal, 64, 520–522.

Wu, C.C., Kumarakrishnan, S., and Mason, T.O. (1981) Thermopower composition dependence in ferrospinels. Journal of Solid State Chemistry, 37, 144–150.

Yagnik, C.M., and Mathur, H.B. (1968) A Mössbauer and X-ray diffraction study on the cation distribution in $FeAl_2O_4$. Journal of Physics C, Solid State Physics, 1, 469–472.

Manuscript received December 17, 1987
Manuscript accepted November 23, 1988